



1 **Multiscale assessment of TRMM (3B42 V7) and GPM**
2 **(IMERG V5) satellite precipitation products over a**
3 **Mediterranean mountainous watershed with sparse rain**
4 **gauges in the Moroccan High Atlas (case study of Zat basin)**

5 Myriam Benkirane ^{1,*}, Nour-Eddine Laftouhi ¹, Said Khabba², Bouabid El Mansouri³

6 ¹ GeoSciences Laboratory, Geology Department, Faculty of Sciences Semailia, Cadi Ayyad University (UCAM),
7 Marrakech, Morocco

8 ² Joint International Laboratory TREMA, Physics Department, Faculty of Sciences Semailia, Cadi Ayyad
9 University, (UCAM), Marrakech, Morocco

10 ³ Natural Resources Geosciences Laboratory, Geology Department, Faculty of Sciences, Ibn Tofail University,
11 Kenitra, Morocco

12

13 *Correspondence to:* Myriam Benkirane (myriam14.benkirane@gmail.com)

14

15 **Abstract.** The performance of Tropical Precipitation Measurement Mission (TRMM) and its successor, Global
16 Precipitation Measurement (GPM), has provided hydrologists with a source of critical precipitation data for
17 hydrological applications in basins where ground-based observations of precipitation are sparse, or spatially
18 undistributed.

19 The very high temporal and spatial resolution satellite precipitation products have therefore become a reliable
20 alternative that researchers are increasingly using in various hydro-meteorological and hydro-climatological
21 applications.

22 This study aims to evaluate statistically and hydrologically the TRMM (3B42 V7) and GPM (IMERG V5) satellite
23 precipitations products (SPPs), at multiple temporal scales from 2010 to 2017, in a mountainous watershed under
24 a Mediterranean climate.

25 The results show that TRMM (3B42 V7) and GPM (IMERG V5) satellite precipitation products have a significant
26 capacity for detecting precipitation at different time steps. However, the statistical analysis of SPPs against ground
27 observation shows good results for both statistical metrics and contingency statistics with notable values ($CC >$
28 0.8), and representative values relatively close to 0 for the probability of detection (POD), critical success index
29 (CSI), and false alarm ratio (FAR). Moreover, the sorting of the events implemented on the hydrological model
30 was performed seasonally, at daily time steps. The calibrated episodes showed excellent results with Nash-Sutcliffe
31 values ranging from 53.2% to 95.5%.

32 Nevertheless, the (IMERG V5) product detects more efficiently precipitation events at short time steps (daily),
33 while (3B42 V7) has a solid ability to detect precipitation events at large time steps (monthly and yearly).
34 Furthermore, the modeling results illustrate that both satellite precipitation products tend to underestimate
35 precipitation during wet seasons and overestimate them during dry seasons, while they have a better spatial
36 distribution of precipitation measurements performance, which shows the importance of their use for basin
37 modeling and potentially for flood forecasting in Mediterranean catchment areas.

38 **Keywords:** Satellite precipitation, Rain gauge, Precipitation, Evaluation, Mediterranean climate, Hydrological
39 modeling, Zat watershed.



40 1. Introduction

41 Precipitation is a major force in global climate change and plays an important role in hydrological and
42 meteorological applications (Yuan *et al.*, 2017). As a significant phenomenon in nature; precipitation has complex
43 characteristics of spatiotemporal variations. It is one of the critical components of the global exchange of the
44 surface material, the hydrological cycle, and disaster prevention (Bollasina *et al.*, 2011; Zhu *et al.*, 2012).

45 The variability of precipitation in mountainous areas directly affects local agriculture and ecological environment
46 (Xia *et al.*, 2015; Jiang *et al.*, 2017). Moreover, the heavy precipitation events that occurred in mountainous areas
47 frequently generate flash floods (Borga *et al.*, 2010). Therefore, the acquisition of reliable and accurate
48 precipitation information in mountainous areas is of great significance to social and economic development and
49 related scientific researches (Germann *et al.*, 2006). Rain gauge observation could provide a moderately accurate
50 method for point-based precipitation measurement. However, rain gauges in mountainous regions are often scarce,
51 irregular, and sometimes unavailable (Xia *et al.*, 2015; Hrachowitz *et al.*, 2011). Thus, in the applications that need
52 high spatiotemporal resolution precipitation data, such as flood disaster forecasts, gauge data are regularly
53 insufficient (Mei *et al.*, 2014; Yi *et al.*, 2018). Contrary to rain gauge precipitations, satellite remote sensing has
54 the advantages of completely scanning the entire study region and convenient access to the data, providing an
55 alternate way to monitor precipitation at regional and global scales (Chen *et al.*, 2018).

56 In recent decades, a series of high spatiotemporal resolutions Satellite Precipitation Products (SPPs), have been
57 produced with the development of various space borne and related satellite-based precipitation retrieval
58 algorithms, such as Artificial Neural Networks (PERSIANN) (Sorooshian *et al.*, 2000), National Oceanic and
59 Atmospheric Administration/Climate Prediction Center (NOAA/CPC) morphing technique (CMORPH) (Joyce *et al.*,
60 2004; Guo *et al.*, 2014), Climate Hazards Group InfraRed Precipitation with Station data (CHIRPS) (Funk *et al.*,
61 2015), Tropical Rainfall Measuring Mission (TRMM) Multi-satellite Precipitation Analysis (TMPA)
62 (Huffman *et al.*, 2007), and Integrated Multi-satellite Retrievals for (GPM) mission (IMERG) (Hou *et al.*, 2014).
63 Compared to these satellite precipitation products, the TRMM 3B42V7 precipitation product performance is higher
64 than other products, especially in estimating extreme precipitation events in several areas around the world (Tong
65 *et al.*, 2014; Ringard *et al.*, 2015). TRMM was launched in November 1997 by the National Aeronautics and Space
66 Administration (NASA) with the collaboration of the Japanese Aerospace Exploration Agency (JAXA). The
67 TRMM Version-7 offers quasi-global coverage (50°N–50°S) precipitation estimates at a high spatial resolution of
68 (0.25° X 0.25°) and temporal resolution of 3 hours (Huffman *et al.*, 2007).

69 Given the excellent successes of the TRMM, the GPM Core Observatory satellite was set in motion by NASA and
70 JAXA as a successor of TRMM in February 2014. Compared with TRMM, the potential of GPM to detect liquid
71 and solid precipitation is improved by carrying space-borne dual-frequency precipitation radar (Chandrasekar *et al.*,
72 2015). Additionally, the GPM Core Observatory carrying a conical scanning multichannel microwave imager
73 offers a wider measurement range (Hou *et al.*, 2014). The lately released IMERG further expands quasi-global
74 coverage from (50°N–50°S) to (60°N–60°S) and provides precipitation estimates with a finer spatial resolution of
75 (0.1° X 0.1°) and temporal resolution of 30 minutes (Liu *et al.*, 2017).

76 Since the deliverance of IMERG products, Many studies have been conducted to evaluate and compare the
77 performance of TMPA and IMERG products regarding rain gauges observations in many regions, such USA
78 (Gebregiorgis *et al.*, 2018), Brazil (Rozante *et al.*, 2018), Japan (Kim, *et al.*, 2017), China (Zhong *et al.*, 2019),
79 South Korea (Wu *et al.*, 2017), Malaysia (Tan *et al.*, 2018), Pakistan (Hussain *et al.*, 2018), South America



80 (Palomino-Ángel, et al., 2019), Cyprus (Retalis *et al.*, 2018), Egypt (Saber et al., 2015), and Morocco (Milewski
81 et al., 2015; Milewski et al., 2020). However, most of these studies indicate that IMERG had greater performance
82 in the characterization of precipitation variability and precipitation detection aptitude, with the only slight
83 improvement compared to TMPA products.

84 This study statistically and hydrologically evaluated GPM (IMERG V5) and TRMM (3B42 V7) satellites
85 precipitation estimates comparatively to ground precipitation observations over Zat semi-arid mountainous
86 watershed located in the Moroccan High Atlas. The objectives are to (1) Assess and statistically compare the
87 performance of IMERG V5 and 3B42 V7 precipitation products at multiple temporal scales in the Zat basin, (2)
88 Analyze the precipitation detection ability of 3B42 V7 and IMERG V5 satellite sensors and (3) Evaluate the ability
89 of the SPPs to reproduce rainfall events and demonstrate their aptitude to provide meaningful information in
90 hydrological modelling and flood forecasting.

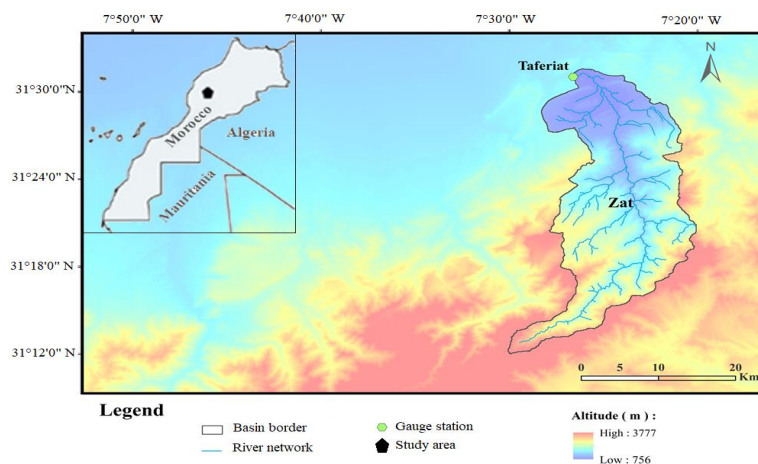
91 This manuscript provides a valuable reference for monitoring and forecasting precipitation in mountainous regions
92 characterized by a Mediterranean climate, as well as basins where rainfall stations are scarce or poorly distributed.

93 2. Study Area and Datasets

94 2.1. Study area

95 Zat watershed is a sub-basin of the Tensift catchment, it's also an Atlas tributary located on the left bank of Tensift
96 river and situated in the Moroccan High Atlas Mountains (Mount Toubkal, the highest mountain in North Africa),
97 in the South EST of Marrakech city. Geographically the sub-basin is found between latitude 31°30' and 31°45'
98 North and longitude 7°30' and 7°45' West. It's drained by the Zat River, which measures 89 km, the slopes are
99 often very steep with an average of 19%, and it covers a total area of about 519 km² (Figure 1). The topography of
100 the catchment area varies from 3777 m (above sea level) downstream to the Taferiat station where the outlet is at
101 an altitude of 756 m. (Benkirane *et al.*, 2020).

102 This sub-basin is characterized by Mediterranean climate strongly influenced by altitude. Taferiat hydrometric
103 station controls the discharge of the Zat Basin, and also serves as rain gauge. It receives an annual rainfall average
104 ranges from 133 mm /year to 913 mm /year; precipitation is mainly concentrated during the rainy period from
105 October to April and a hot and dry period from May to September. Therefore, this study region is subject to
106 frequent flash floods and droughts.





108 **Figure 1. The geographical location of the Zat basin and rain gauge station used in the study.**

109 2.2. Rain gauge data

110 Rain gauge measurements are daily precipitation data collected from only one meteorological station shown in
111 (Figure. 1) located at the outlet of Zat basin, covering a period from 2010 to 2017. Data sets are provided by the
112 Tensift Hydraulic Basin Agency. These data were used as a benchmark for evaluating TRMM (3B42 V7) and
113 GPM (IMERG V5) SPPs. All observations provided by these stations are subject to strict quality control such as
114 climate limit value inspection, and station extreme value inspection (Shen *et al.*, 2018). In addition, the monthly
115 and yearly precipitation values are accumulated from daily observations.

116 2.3. Satellite precipitation data

117 This study evaluated two types of satellite precipitation products (SPPs), the TRMM (3B42 V7), and the GPM
118 (IMERG V5) at different time scales, from September 01 2010 to August 31 2017 (Table1). Before accumulating
119 the dataset from daily to monthly and yearly precipitation, both products were converted from UTC to UTC +1 to
120 unify the time with the study area (Wang *et al.*, 2019), a brief description of these SPPs is given as follows.

121 **Table 1. Main parameters of TRMM (3B42 V7) and GPM (IMERG V5) satellite precipitation products.**

Satellite precipitation products	TRMM (3B42 V7)	GPM (IMERG V5)
Temporal / Spatial Resolutions	3 h /0.25°	0.5 h /0.1°
Coverage Period	December 1997 to Present	March 2014 to Present
Coverage Range	Global (50°N–50°S)	Global (60°N–60°S)

122 2.3.1. TRMM (3B42V7)

123 The TRMM (3B42 V7) precipitation products were generated by using the TRMM 3B42 Version 7 algorithm
124 (Huffman *et al.*, 2007). It was designed to combine various microwaves MW, and infrared IR satellite-based
125 precipitation estimates with gauge adjustments observations to provide 3-hourly quasi-global quantitative
126 precipitation estimates (Hou *et al.*, 2014). The 3B42 V7 product is derived by bias-adjusting the near-real-time
127 product with the GPCC monthly gauge-analysis precipitation data set, and it has two-month latency (Yuan *et al.*,
128 2017). The product can produce rational precipitation estimates in a 0.25° spatial resolution with a quasi-global
129 coverage (50°S–50°N). In this study, the TRMM 3B42 V7 daily precipitation product was acquired from the
130 Precipitation Measurement Mission (PMM) website (<https://pmm.nasa.gov/data-access/downloads/trmm>).

131 2.3.2. GPM (IMERG V5)

132 The GPM project is the result of collaboration between (NASA) and (JAXA). GPM satellite carries two primary
133 sensors: The multi-channel GPM Microwave Imager (GMI), and the Dual-frequency Precipitation Radar (DPR).
134 This satellite product is expected to provide the next-generation global observations of rain and snow and to
135 improve weather and precipitation forecasts through the assimilation of instantaneous precipitation information
136 (Kim *et al.*, 2017). IMERG is the Level 3 precipitation estimation algorithm of GPM, it provides three different
137 daily IMERG products, which include IMERG Day 1 Early Run (near real-time with a latency of 6 h), IMERG
138 Day 1 Late Run (reprocessed near real-time with a latency of 18 h) and IMERG Day 1 Final Run (gauged-adjusted
139 with a latency of four months) products (Chen *et al.*, 2018). In this study, we evaluate the latest released GPM
140 IMERG Version 5 (IMERG V5), the dataset is produced at NASA Goddard Earth Sciences (GES). The IMERG
141 precipitation products have a relatively finer spatial 0.1°spatial resolution with spatial coverage from 60°S to 60°N
142 and temporal (half-hourly) resolution. The daily precipitation data were accumulated to obtain monthly and annual



143 precipitation. The GPM (IMERG V5) precipitation data were downloaded from the PMM website
 144 (<https://pmm.nasa.gov/data-access/downloads/trmm>).

145 2.4. Methodologies

146 Different methods were used to compare the IMERG V5 and 3B42 V7 products with the gauge precipitation data
 147 from the Taferiat station, depending on the time steps considered (daily, monthly, and annual). However, the
 148 satellite products represent the rainfall estimates at the scale of (0.1 ° for IMERG V5 and 0.25 ° for 3B42 V7,
 149 respectively), while the gauge precipitation observed represents precipitation on a point scale. For comparison, the
 150 method frequently used is to increase the point precipitation data from the gauges to the same grid scale as the
 151 SPPs, either by spatial interpolation or simply by calculating the average. In addition, the researchers pointed out
 152 that the interpolation can lead to uncertainties due to systematic error and the density of the gauge (Duan *et al.*,
 153 2016). Therefore, a direct comparison is used in this study. To evaluate these two SPPs, we only considered the
 154 grids that cover the data of the single gauging station present in the Zat basin. Therefore, the grids not covering
 155 the gauge station were excluded from the assessment.

156 Furthermore, to evaluate the ability of the SPPs to reproduce rainfall events, it was decided to use them as input
 157 data in a surface hydrological model, the HEC-HMS model. Indeed, the rainfall measurement stations are not
 158 precise and poorly distributed spatially, especially in the mountainous regions of the High Atlas, which is a real
 159 issue for research work on hydrological modeling and flood forecasting. Consequently, it is important to evaluate
 160 the rainfall estimated by the satellites to demonstrate their ability to provide significant information and to approve
 161 their use as an alternative source of rainfall measurement data

162 2.4.1. Statistical Evaluation of Satellite Precipitation Products

163 Several diagnostic indices were used to statistically assess the quality of IMERG V5 and 3B42 V7 products
 164 compared to observations of ground precipitation. Indeed, the comparison was carried out based on a general
 165 evaluation (continuous statistical measurements) and of the precipitation detection capacity (categorical statistical
 166 measurements) (Table 2).

167 Continuous statistical indices

168 Four statistical measures were selected, including correlation coefficient (CC), root mean square error (RMSE),
 169 relative bias (RB), and bias (bias), which were calculated to statistically evaluate the two PPS products.
 170 The Pearson Correlation Coefficient (CC) measures the agreement between the PPS products and the gauge data.
 171 The (RMSE) was used to represent the mean magnitude of the error. The (RB) and (bias) was applied to evaluate
 172 the systematic bias between the SPPs and gauge data in percent and amount of precipitation, respectively. The
 173 overestimation of the precipitation estimate is represented by positive (RB) or (Bias) values, and vice versa.

174 **Table 2. Statistical metrics for evaluating IMERG V5 and 3B42 V7 products**

Statistical Index	Units	Equation
Correlation Coefficient (R)	Ratio	$CC = \frac{\sum_{i=1}^N (P_i - \bar{P})(S_i - \bar{S})}{\sqrt{\sum_{i=1}^N (P_i - \bar{P})^2 \sum_{i=1}^N (S_i - \bar{S})^2}}$
Root Mean Square Error (RMSE)	mm	$RMSE = \sqrt{\frac{\sum_{i=1}^N (P_i - S_i)^2}{N}}$



Mean Absolute Error (MAE)	mm	$MAE = \frac{\sum_{i=1}^N P_i - S_i }{N}$
Relative Bias (RB)	%	$RB = \frac{\sum_{i=1}^N (P_i - S_i)}{\sum_{i=1}^N S_i} \times 100\%$
Bias	N/A	$Bias = \frac{\sum_{i=1}^N (P_i - S_i)}{\sum_{i=1}^N N}$
Probability Of Detection (POD)	Ratio	$POD = \frac{a}{a + c}$
False Alarm Ratio (FAR)	Ratio	$FAR = \frac{b}{a + b}$
Critical Success Index (CSI)	Ratio	$CSI = \frac{a}{a + b + c}$
Frequency Bias Index (FBI)	Ratio	$FBI = \frac{a + b}{a + c}$

175

176 Where N represents the number of samples; S_i and \bar{S} are gauge observations and their average; P_i and \bar{P} represent
 177 satellite estimates and their average, respectively.

178 Also, a, denotes the number of rainfall events that observed and detected; c, is the number of rainfall that failed to
 179 be detected by the satellite; b, denotes the number of rainfall events detected by the satellite that did not occur; the
 180 threshold for identifying a precipitation event is 0.5 mm/day.

181 **Categorical statistical indices**

182 To evaluate the precipitation detection capability of IMERG V5 and 3B42 V7 products, four categorical statistical
 183 indices were calculated to assess the ability of PPSs. The most common measures, counting Probability of
 184 Detection (POD), False Alarm Rate (FAR), Critical Success Index (CSI), and Frequency Bias Index (FBI) are used
 185 in this study. The values of all categorical statistical measures are between 0 and 1.

186 The POD indicated the ratio of the number of precipitation events correctly detected by satellites among all real
 187 precipitation events. The FAR is the ratio of false alarming precipitation events to the total number of detected
 188 precipitation events. The FBI represents the fraction of falsely detected precipitation events (false alarm) compared
 189 to the total number of detected precipitation events, it indicates whether the dataset tends to overestimate (FBI > 1)
 190 or underestimate (FBI < 1) precipitation events. The CSI reported the number of correct predictions of a rain event
 191 divided by the total number of successes, false alarms, and failures. Table 3 shows the formulas for these metrics.

192

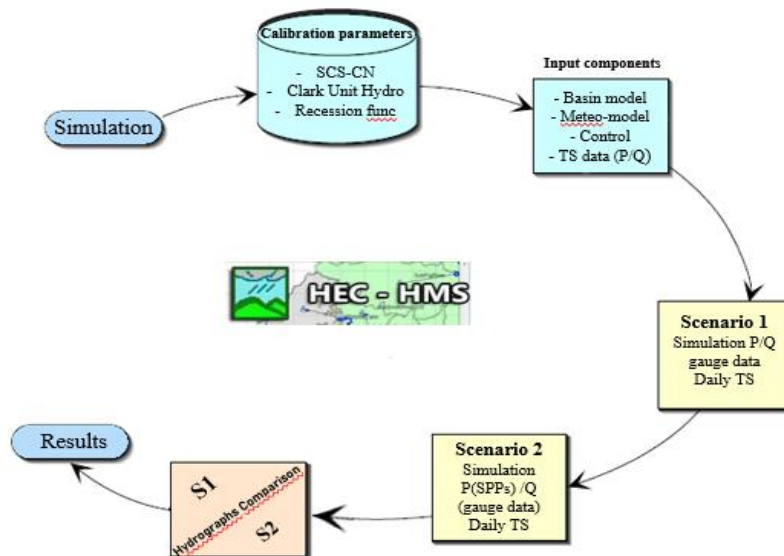
Table 3. Contingency table to evaluate precipitation occurrence by satellite products

		Satellite	
		Rain (daily rain ≥ 0.5 mm)	No rain (daily rain <0.5 mm)
Gauge	Rain (daily rain ≥ 0.5 mm)	a: hits	b: false
	No rain (daily rain <0.5 mm)	c: misses	d: correct negatives



193 Hydrological Model

194 The Hydrologic Engineering Centre's Hydrologic Modeling System (HEC-HMS) is designed to simulate the
195 rainfall-runoff processes of dendritic watershed systems. This model is known to be applicable in a wide range of
196 geographic areas for solving the broadest possible range of problems (Scharffenberg and Fleming 2016). The
197 method used in this paper includes SCS-CN (Soil Conservation Service) Curve Number, Clark Unit Hydrograph,
198 and Baseflow Recession, which are necessary to determine the hydrologic loss rate, runoff transformation, and
199 base flow rates. This method aims to calibrate four rainfall events according to seasons (autumn, winter, spring,
200 summer), with a daily time step precipitation by implementing the model with different precipitation data sources
201 such as observed and satellite precipitation with observed runoff to evaluate the ability of the SPPs to reproduce
202 rainfall events according to seasons (Figure. 2).



203

204 **Figure 2. Schematic representing the adopted approach for the hydrological modelling research.**

205

205 3. Results

206

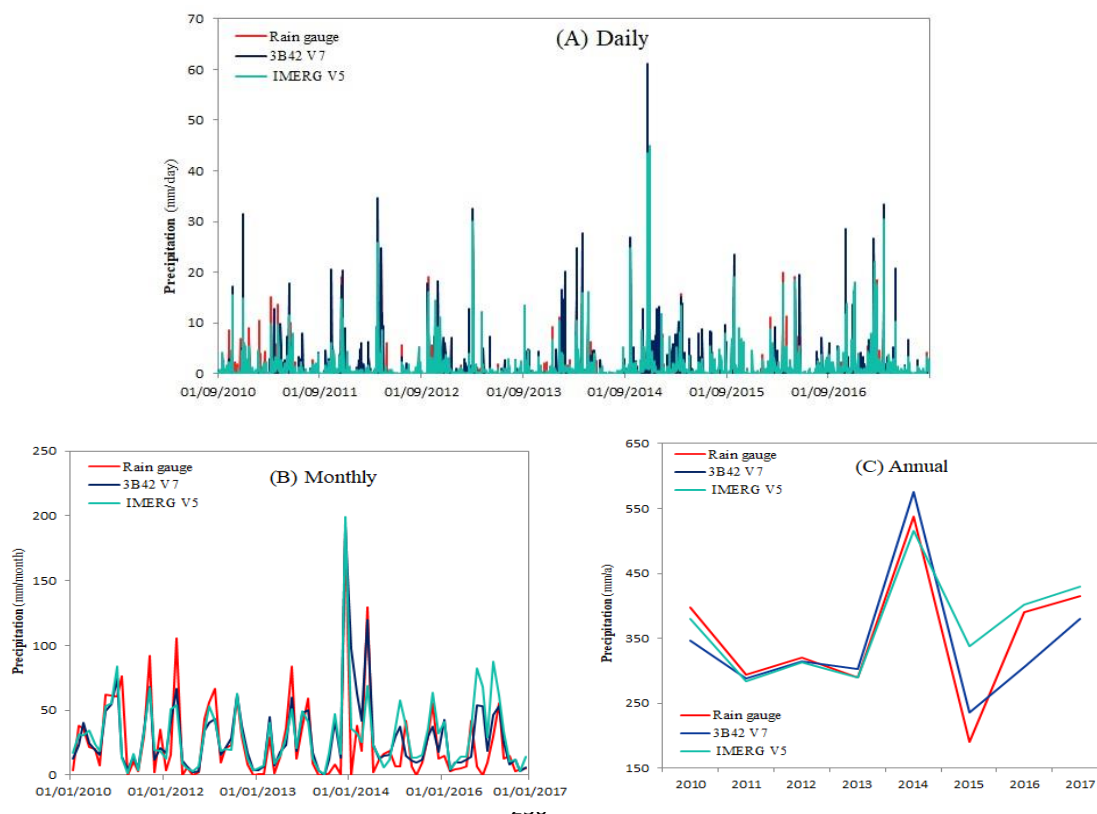
206 3.1. Assessment of precipitation at a different time scale

207

207 The rainfall time series of the two selected satellite products and the rain gauge at different timescales in the Zat
208 basin are presented in (Figure 3). In general, the 3B42 V7 and IMERG V5 products present similar chronological
209 precipitation patterns to those of the gauge. However, it can be seen that the product 3B42 V7 slightly
210 overestimated the daily precipitation, while the product IMERG V5 showed good performance on the daily
211 timescale (Figure 3A). Regarding the monthly precipitation series, the product 3B42 V7 underestimated the
212 monthly precipitation, while IMERG V5 clearly showed good initial agreement with the observed precipitation,
213 although from 2015 IMERG V5 slightly overestimated the monthly precipitation (Figure 3B). As for the annual
214 time scale, the precipitation series was overestimated by the precipitation products 3B42 V7 and IMERG V5, this
215 phenomenon is similar to that of the monthly scale, the overestimation was observed from 2015 onward (Figure
216 3C).



217
 218
 219
 220
 221
 222
 223
 224
 225
 226
 227
 228
 229
 230
 231
 232
 233
 234
 235



237
 238
 239

Figure 3. Precipitation time series from rain gauges, 3B42 V7, and IMERG V5, in the Zat basin from 2010 to 2017 (a, Daily; b, Monthly; c, Annual).

240

3.2. Statistical evaluation

241

The SPPs were statically compared against the ground observations to evaluate their accuracy and reliability.

242

Table 4. Lists the evaluation results of statistical metrics (CC, RMSE, MAE, R Bias, and Bias), thought the

243

entire study period over the Zat basin.

244

Table 4. Statistical metrics results of 3B42 V7 and IMERG V5 precipitation estimates at multiple time scales from 2010 to 2017.

245

	TRMM			GPM		
	Daily	Monthly	Yearly	Daily	Monthly	Yearly
CC	0.78	0.80	0.90	0.81	0.75	0.85
RMSE	2.03	19.90	42.84	1.68	22.09	53.64
MAE	0.71	12.85	34.72	0.62	14.49	29.03
R Bias	29.48	16.47	- 2.99	47.13	21.73	4.07
Bias	0.19	4.14	- 10.61	0.31	5.46	14.44

246

Figures 4 and 5. Shows the scatterplots and boxplots with the statistical metrics for the 3B42 V7 and IMERG V5

247

products versus ground-based rain gauge observation. The scatterplots of SPPs products against rain gauge

248

precipitation exhibit a concentration of the points near the 1:1 line especially at daily and monthly scales.

249

According to the metrics plotted in Figures 4 and 5 (A), 4 and 5 (B), and 4 and 5 (C), the performance of the

250

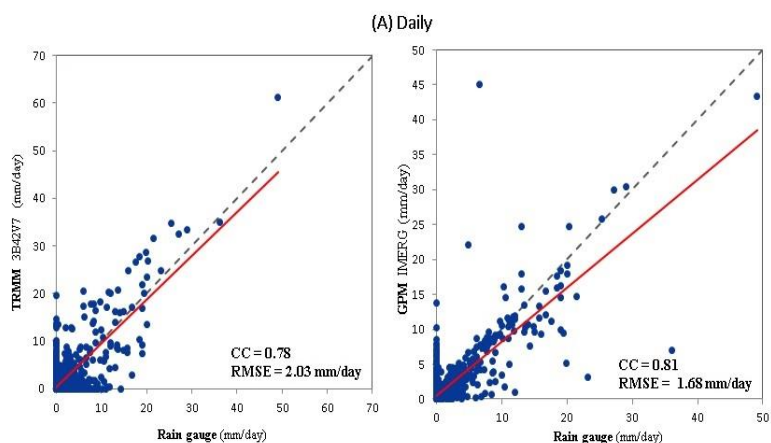
IMERG V5 is superior to that of the 3B42 V7 at daily scale. However, the obtained results at monthly and yearly

251

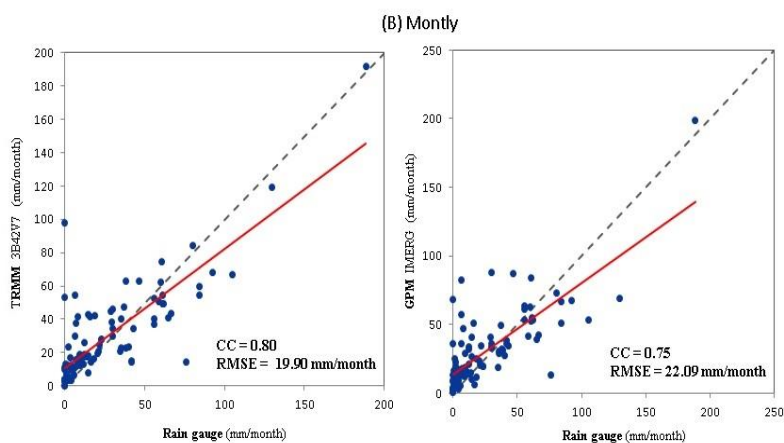
scales for the 3B42 V7 are significantly better than IMERG V5.



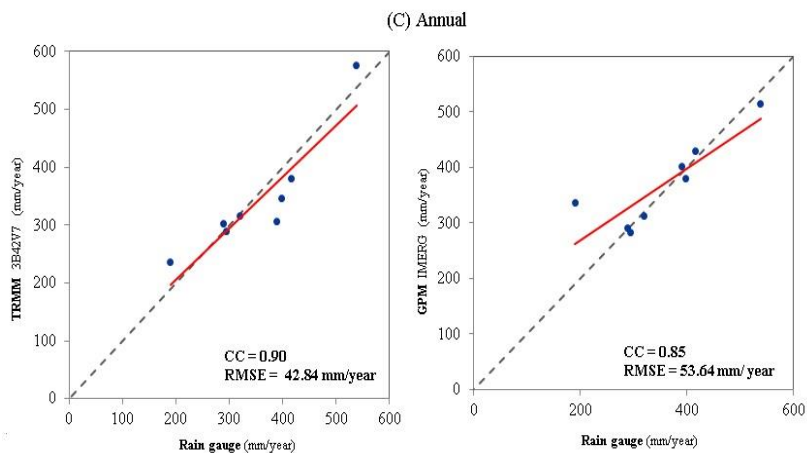
252



253



254



255

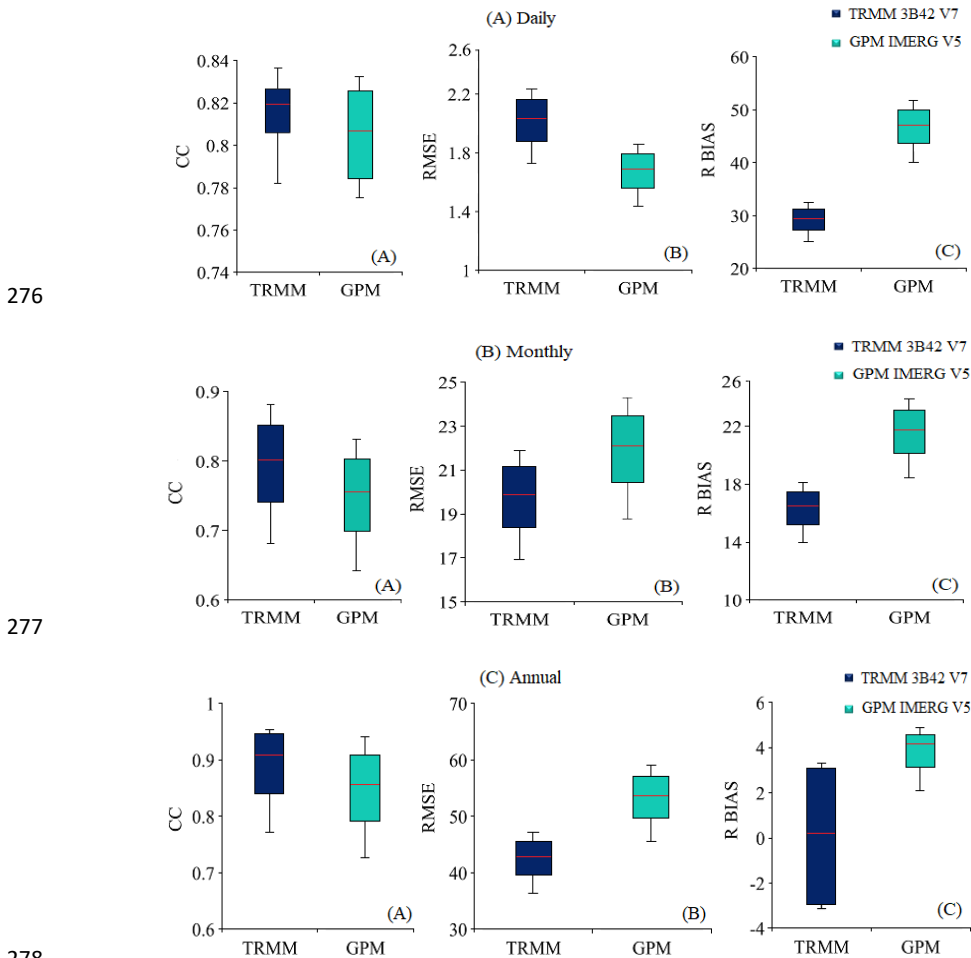
Figure 4. Scatterplots for TRMM3B42 v7 and GPM IMERG v5 precipitation versus ground-based rain gauge measurements over the Zat watershed "(A–C) daily, monthly, and annual scales, the black and red oblique lines denote a 1 : 1 line and a least-squares regression line, respectively".

256

257



258 Both 3B42 V7 and IMERG V5 products present a strong correlation with gauge data at a daily scale. Figure 4 A
 259 shows a high CC (0.78) and (0.81) respectively a small RMSE error values (2.03 mm) and (1.68mm) respectively,
 260 and relatively balanced R Bias and Bias (29.4%), (0.19) for 3B42 V7 and (47.13%), (0.31) for IMERG V5. In
 261 general, except for the R Bias and the Bias values, the other continuous statistical indices from both products had
 262 good results, and it can be seen that IMERG V5 indices were better than 3B42 V7 at the daily scale Figures (3 and
 263 4 A). Figures (4 and 5 B), Represents scatterplots and boxplot of precipitation from 3B42 V7 and IMERG V5 at
 264 monthly scale. Compared with gauge data, it can be seen that both products slightly underestimate the precipitation.
 265 However, 3B42V7 show a much better correlation with gauge precipitation than IMERG, with higher CC (0.80)
 266 and (0.75), low RMSE (19.90 mm vs. 22.09mm), acceptable MAE (12.85) and (14.42), and relatively low values
 267 of R Bias and Bias (16.47% vs. 21.73%) and (4.14 vs. 5.46) respectively. Meanwhile, 3B42 V7 performed better
 268 than IMERG V5 on a monthly scale. According to the scatterplots and boxplot illustrated in Figures (3 and 4 C),
 269 it can be noticed that the 3B42 V7 product is obviously manifested by a slight underestimation and that the major
 270 performance of the IMERG V5 product is moderately superior to that of 3B42 V7, except at the value of CC and
 271 RMSE. The illustration of both 3B42 V7 and IMERG V5 present a strong correlation with high CC values of
 272 (0.90) and (0.85), low RMSE error (42.84 mm) and (53.64mm), small MAE (34.72) and (29.03), and relatively
 273 good R Bias and Bias (-2.99% vs. 4.07%) and (-10.61 and 14.44) respectively. For the R Bias and Bias, the negative
 274 deviation of 3B42 V7 precipitation estimates was relatively balanced, while IMERG V5 showed a positive
 275 deviation at the rain gauge. Indeed, IMERG V5 showed better performance than 3B42 V7 at a yearly time scale.





279 **Figure 5. Boxplot of correlation coefficient (CC), root mean square error (RMSE), and relative bias (R BIAS) between**
 280 **satellite-based and rain gauge at multiple time scales in Taferiat gauge station, during the period of September 1st to**
 281 **August 31, 2010–2017.**

282 **3.3. Contingency Statistics**

283 The categorical statistical metrics of 3B42 V7 and IMERG V5 at different time scales are shown in (Table 5).

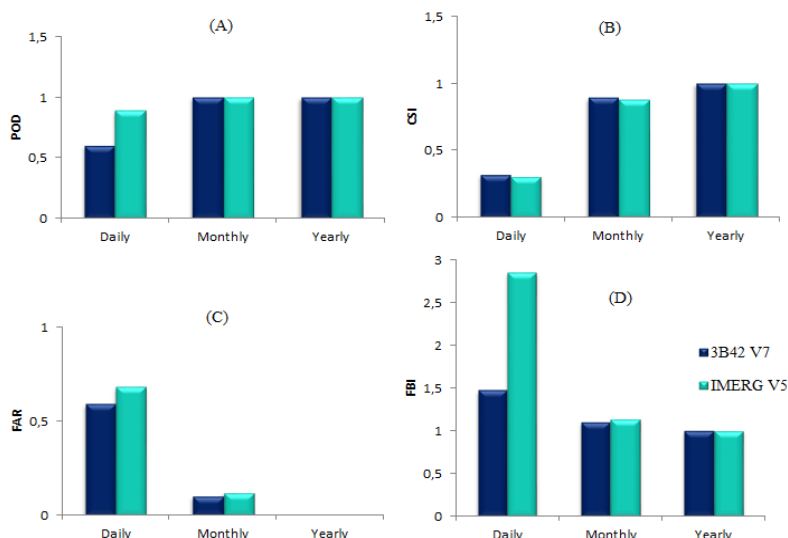
284 **Table 5. Contingency statistical metrics results of 3B42 V7 and IMERG V5 precipitation estimates at multiple time**
 285 **scales from 2010 to 2017.**

	TRMM			GPM		
	Daily	Monthly	Yearly	Daily	Monthly	Yearly
POD	0.6	1	1	0.89	1	1
FAR	0.59	0.1	0	0.68	0.12	0
CSI	0.32	0.89	1	0.33	0.88	1
FBI	1.47	1.1	1	2.85	1.13	1

286 The precision of 3B42 V7 and IMERG V5 at daily, monthly and annual scales was compared and analyzed.
 287 IMERG V5 demonstrated better performance than 3B42 V7 in detecting precipitation events on a daily scale, with
 288 low values of POD and CSI (0.89 vs. 0.6) and (0.33 vs. 0.32) (Figure 5 A, B), as well as reasonably high values
 289 of FAR and FBI (0.68 vs. 0.59) and (2.85 vs. 1.47) respectively (Figure 5 C, D).

290 The performance of the categorical statistical measures at the monthly level is shown in Figure 5. 3B42 V7, and
 291 IMERG V5, produced good results for rainfall estimation, with POD values and CSI approximately similar to the
 292 perfect values in Table 2, the respective values are (1 vs. 1) and (0.89 vs. 0.88) (Figure 5 A, B). Similarly for the
 293 FAR and FBI the results obtained are close to the perfect values, (0.1 vs. 0.12) and (1.1 vs. 1.13) respectively
 294 (Figure 5 C, D).

295 Regarding annual performance, IMERG V5 and 3B42 V7 products show very good results, the performance of
 296 the POD is consistent with that of the CSI, which exhibits perfect values (1 vs. 1) and (1 vs. 1) (Figure 6 A, B) and
 297 similarly, for the FAR and FBI (0 vs. 0) and (1 vs. 1) respectively (Figure 5 C, D), the values are perfectly adequate
 298 to those of Table 2.



299

300 **Figure 6. Metrics results of different time scales (A) POD, (B) CSI, (C) FAR, and (D) FBI, of 3B42 V7 and**
 301 **IMERG V5 products.**



302 In general, IMERG V5 is better at detecting precipitation events, in particular at capturing precipitation traces and
 303 solid precipitation at a daily scale, while 3B42 V7 can estimate precipitation on a large time scale.

304 **4. Hydrological evaluation of discharge simulation using two SPPs.**

305 The HEC-HMS model was used to calibrate the daily rainfall events from (1/09/2010) to (31/08/2017) according
 306 to the different seasons, at the level of the Zat basin, using the rainfall and Runoff data from the Taferiat gauge
 307 station, and satellite precipitation products, the four episodes that we chose to present are the three most
 308 representative of the data series. The hydrological simulations were carried out according to two different
 309 scenarios:

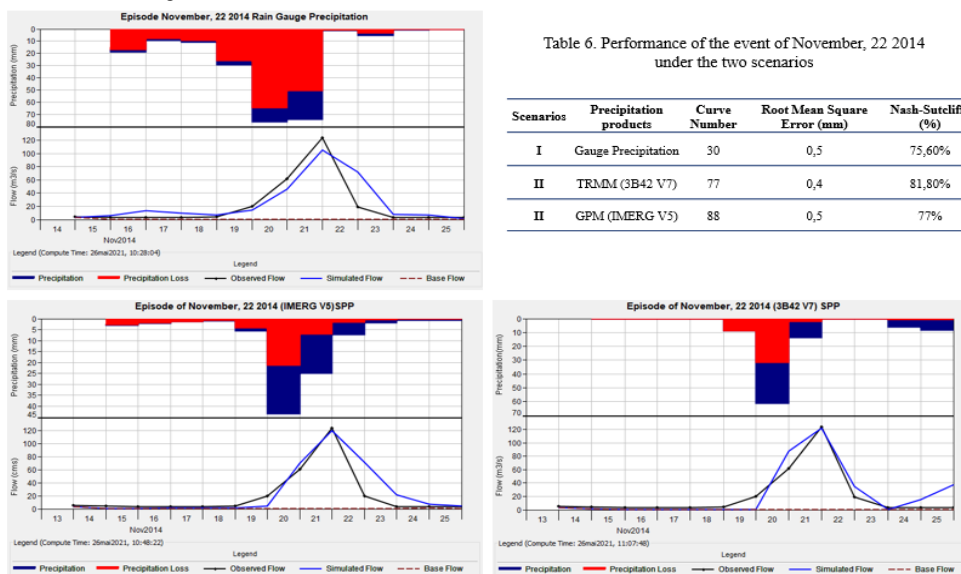
310 Scenario 1: Simulation and calibration by implementing the model with observed rainfall and discharge data.

311 Scenario 2: Simulation and calibration using rainfall from both satellite products with observed flows.

312 **4.1 Event of November 22nd, 2014 (autumn)**

313 This event represents a torrential flood; since the flood was generated by extreme precipitation spread over more
 314 than 15 days, it is the most intense event in the data set. The maximum flow reached is (123,75 m³/s). However,
 315 the soils were saturated, resulting in high permeability and an increase in the runoff coefficient of the watershed.
 316 The results of the simulation and calibration of the rainfall data and the observed flow in the hydrograph of scenario
 317 1 (Figure 6), show that the simulated flow curve was well reproduced both at the flood rise and the recession part,
 318 although the peak flow was not reached, the evaluation criteria are very satisfactory: RMSE = 0.5 and Nash =
 319 75.60%. Scenario 2 represents the results of the simulations and event calibrations with the implementation of the
 320 model with the previously analyzed satellite precipitation products (IMERG V5, 3B42 V7) and the observed flows.
 321 Hydrographs were well reproduced for both the rise and the recession; peak flows were achieved and evaluation
 322 criteria are very satisfactory with RMSE of 0.5 and 0.4 and Nash of 77% and 81.11% respectively.

323 The simulation results of scenario 2 are better than those of scenario 1. This is explained by the fact that the
 324 satellites have several measuring stations well distributed spatially while the Zat basin has only one measuring
 325 station downstream (Taferiat station). In addition, a significant underestimation was found during the analysis of
 326 the 2 SPP data compared to the observed data, this underestimation was compensated by using the elevation of the
 327 curve number during the calibration of the event.



328
 329
 330
 331

Figure 7. Simulation of the episode of November, 22 2014, using rainfall and runoff gauge data as input (Scenario I), and SPPs with measured flow data as input (Scenario II).

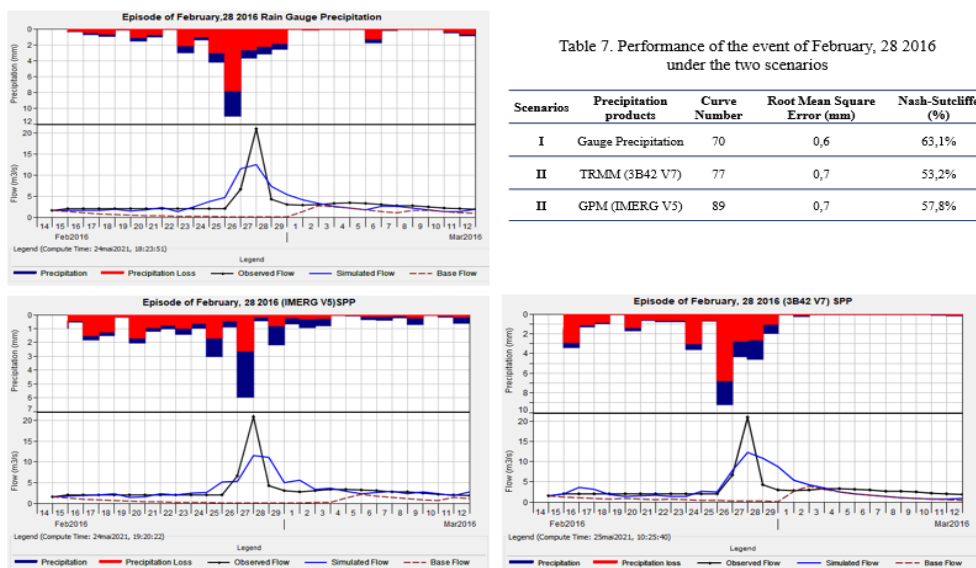


332 **4.2 Event of the February 28, 2016 (winter)**

333 The event represents a winter rain storm characterized by liquid precipitation downstream and snow upstream of
 334 the watershed. This type of rain storm is very frequent during the winter, especially in the high mountains of the
 335 Atlas.

336 The hydrograph of scenario 1 represents a simulated flow curve quite illustrative, the rising curve and the recession
 337 were well reproduced, contrary to the peak flow which has not been reached, the evaluation criteria are moderately
 338 good representing values of RMSE = 0.6 and Nash = 63.1%, this is induced by the fact that the snowy fraction has
 339 not been taken into account due to the irregularity of the precipitation measuring stations.

340 On the other hand, the hyetogram of scenario 2 illustrates a good spatial distribution of precipitation, although the
 341 curves of the simulated flows are quite well reproduced, and the peak flows were not reached, the evaluation
 342 criteria are acceptable with RMSE of 0.7 for IMERG V5 and 3B42 V7 and Nash of 57.8% and 53.2% respectively.
 343 Given this, an intense underestimation of the precipitation was noticed while obtaining the calibration results,
 344 which are mainly related to the fraction of snow precipitation not considered.
 345



346
 347 **Figure 8. Simulation of the episode of February, 28 2016, using rainfall and runoff gauge data as input (Scenario I),**
 348 **and SPPs with measured flow data as input (Scenario II).**

349 **4.3 Event of May 02, 2011 (spring)**

350 This event represents the typical characteristics of a freshet caused by the melting of snowfall upstream of the Zat
 351 watershed during the winter, with the progressive increase of temperatures during the spring the snow cover at the
 352 summit of the Atlas Mountains start melting and feed the streams of the mountainous basins including the study
 353 basin. This usually causes significant flooding during the occurrence of moderate rainfall episodes. The
 354 hydrograph of scenario 1 is perfectly calibrated, the simulated flow curve was well reproduced at the rise and at
 355 the recession, the peak flow was reached, and the evaluation criteria are excellent with an RMSE of 0.2 and a Nash
 356 of 95.5%. On the other hand, the hydrographs of scenario 2 are perfectly reproduced at both rising and recession
 357 parts, the peak flow has been reached, the evaluation criteria are excellent with an RMSE of 0.2 for the product
 358 (IMERG V5) and 0.3 for (3B42 V7), and a Nash of 87% and 73% respectively. Indeed, the overestimation of
 359 precipitation generated by the satellite products was compensated by the flows produced by the snowmelt, which
 360 allowed the model to reproduce this event well. It is essential to mention that the SPP overestimates precipitation
 361 during warm seasons.

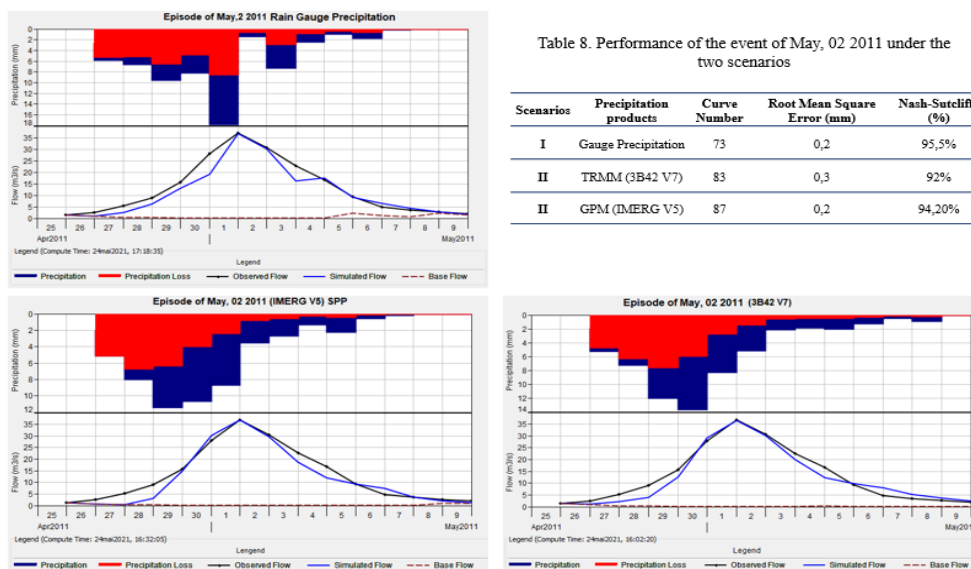


Table 8. Performance of the event of May, 02 2011 under the two scenarios

Scenarios	Precipitation products	Curve Number	Root Mean Square Error (mm)	Nash-Sutcliffe (%)
I	Gauge Precipitation	73	0,2	95,5%
II	TRMM (3B42 V7)	83	0,3	92%
II	GPM (IMERG V5)	87	0,2	94,20%

362
 363
 364

Figure 9. Simulation of the episode of May, 02 2011, using rainfall and runoff gauge data as input (Scenario I), and SPPs with measured flow data as input (Scenario II).

365 **4.4 August 27th, 2011 event (summer)**

366 The summer event of August 27th, 2011, called flash flood, is characterized by a sudden occurrence and short
 367 duration due to stormy precipitation, and initial soil conditions very favourable to runoff. The Atlas watersheds
 368 are mostly dry during the summer due to the high temperatures typical of the Mediterranean climate, and as such
 369 low rainfall can cause dangerous floods.

370 The simulated flow curve of the hydrograph of scenario 1 is well reproduced despite the slight shift located at the
 371 rise and the recession curve, as well as the peak flow that is not reached, the evaluation criteria are satisfactory, an
 372 RMSE of 0.4 and a Nash of 84.30%.

373 The hydrographs of scenario 2 are well reproduced, in particular, that of the SPP (3B42 V7), the evaluation criteria
 374 are satisfactory with an RMSE of 0.4 for (IMERG V5) and 0.3 for (3B42 V7), as well as a Nash of 80.1% and
 375 91.3% respectively.

376 It is important to note that the basin response is relatively slow due to the initial soil conditions, additionally to the
 377 overestimation of precipitation from the satellite products during the high-temperature seasons.

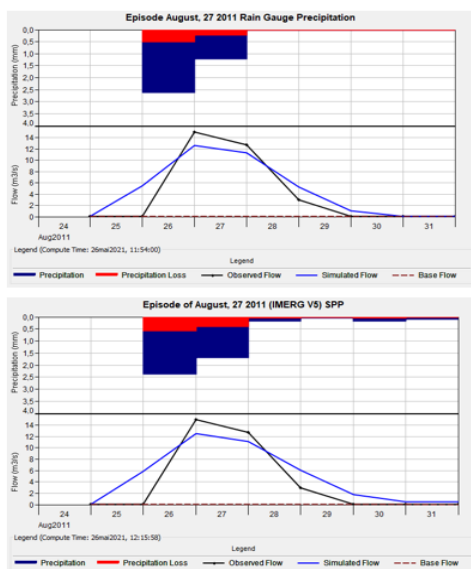


Table 9. Performance of the event of August, 27 2011 under the two scenarios

Scenarios	Precipitation products	Curve Number	Root Mean Square Error (mm)	Nash-Sutcliffe (%)
I	Gauge Precipitation	76	0,4	84,30%
II	TRMM (3B42 V7)	77	0,3	91,3%
II	GPM (IMERG V5)	70	0,4	80,10%

378
 379
 380
 381
 382
 383
 384

Figure 10. Simulation of the episode of August, 27 2011, using rainfall and runoff gauge data as input (Scenario I), and SPPs with measured flow data as input (Scenario II).

This is an efficient method developed in this paper for the first time in a country with a Mediterranean climate, on the mountainous watersheds of the Moroccan High Atlas with low density and irregularity of precipitation and flow measurement stations. This is a good method to apply to solve the problem of deficiency of observed data in these regions.

385 5. Conclusion

386 SPPs are important precipitation data alternatives, particularly in high mountain watersheds, where measurement
 387 gauge stations are poorly distributed or absent. These products will mainly help in the simulation of river flows,
 388 flood forecasting, and water resources management in arid to semi-arid regions. This study conducted a complete
 389 performance evaluation of two satellite products the TRMM (3B42 V7) and the GPM (IMERG V5) using
 390 observations (daily, monthly and annual) collected the only gauge station of the Zat basin, named Taferiat station
 391 and located at the downstream of the watershed. The watershed is characterized by a Mediterranean climate and
 392 mountainous topography, and the study was analyzed over 7 years, from September 01, 2010 to August 3, 2017.
 393 To evaluate the accuracy of 3B42 V7 and IMERG V5 satellite precipitation products, several quantitative,
 394 categorical, and graphical statistical measurements were used, (R, RMSE, MAE, R Bias, Bias) are used to
 395 quantitatively analyze the accuracy of satellite precipitation products, and (POD, CSI, FAR, and FBI) were used
 396 to evaluate the precipitation detection capability of satellite precipitation products, and to simulate satisfactorily
 397 the flooding events in hydrological model.

398 The conclusions resulting from this study are summarized as follows:

- 399 (1) IMERG V5 and 3B42 V7 products performed well in estimating daily, monthly, and annual precipitation
 400 compared to observed data from the Taferiat station. SPPs products slightly underestimated the daily and annual
 401 precipitation, while 3B42 V7 slightly underestimated the monthly precipitation, especially during winter periods.
 402 (2) Compared to the ground applications, 3B42V7 and IMERG V5 showed good correlation results at the daily
 403 scale. However, IMERG V5 performed slightly better than 3B42 V7 for the detection of daily precipitation at the
 404 measuring station. The 3B42 V7 and IMERG V5 products showed a strong correlation with a high CC (0.78) and
 405 (0.81), a small RMSE error value (2.03 mm) and (1.68 mm), and a relatively balanced bias and R-bias (29.4%),
 406 (0.19) and (47.13%), (0, 31) respectively, the POD and CSI values are (1 vs. 1) and (0.89 vs. 0.88), the FAR and
 407 FBI obtained values are (0.1 vs. 0.12) and (1.1 vs. 1.13) respectively, noted that the results of the categorical
 408 measures are good.



409 (3) The performance evaluation results on the monthly scale show good performance of the SPPs. The 3B42 V7
410 show a better correlation with gauge rainfall than IMERG V5, with higher CC (0.80) and (0.75), low RMSE (19.90
411 mm vs. 22.09 mm), acceptable MAE (12.85) and (14.42), and relatively low Bias values (16.47% vs. 21.73%) and
412 (4.14 vs. 5.46) respectively. POD and CSI values are (1 vs. 1) and (0.89 vs. 0.88), FAR and FBI results are (0.1
413 vs. 0.12) and (1.1 vs. 1.13) respectively. However, 3B42 V7 performed better than IMERG V5 on the categorical
414 measures at a monthly scale.

415 (4) Regarding annual performance, the two satellite products followed the trend of rain gauge observations very
416 closely, 3B42 V7 slightly underestimating precipitation. 3B42 V7 and IMERG V5 present a strong correlation
417 with high CC values of (0.90) and (0.85), low RMSE error (42.84 mm) and (53.64mm), small MAE (34.72) and
418 (29.03), and relatively good R Bias and Bias (-2.99% vs. 4.07%) and (-10.61 and 14.44) respectively, for the R
419 Bias and Bias, the negative deviation of 3B42 V7 precipitation estimates were relatively balanced, while IMERG
420 V5 showed a positive deviation at the rain gauge. The values of the POD and the CSI are (1 vs. 1) and (1 vs. 1),
421 the FAR and FBI values are (0 vs. 0), and (1 vs. 1) respectively. These results exhibit perfect values. Indeed,
422 IMERG V5 showed better performance than 3B42 V7 in the statistical measures on an annual time scale.

423 (5) The hydrological simulations and calibration were performed according to two different scenarios; scenario 1
424 aims to run the model with observed rainfall and runoff data, scenario 2 used the SPPs with observed flows. The
425 obtained results are satisfactory for all simulations with different precipitations inputs. The Nash coefficients are
426 very good, ranging from 53.2% to 95.5% for the 3B42 V7, IMERG V5, and observed precipitation respectively.
427 The main point to remember is that both satellite precipitation products tend to underestimate precipitation during
428 wet seasons and overestimate them during dry seasons. The proposed method is an interesting approach to apply
429 for solving the problem of insufficient observed data in the Mediterranean regions.

430 Therefore, the results of this study are of great importance for analyzing the prospect's application of SPPs at
431 different time scale, this paper is one of the first papers developing a comparative approach of satellite rainfall
432 products to observed gauge data in North Africa, they could indeed serve researchers as a reference work both in
433 Morocco and neighbouring countries with similar climates and areas with irregular or sparse rain gauge networks.
434

435 **Acknowledgement:** The authors would like to thank Prof. Adam Milewski (Director of Water Resources &
436 Remote Sensing Laboratory (WRRS), Department of Geology, University of Georgia, United States), who
437 thoughtfully revised this manuscript.

438 This research has been supported by “PRIMA-S2-ALTOS-2018 Managing water resources within Mediterranean
439 agrosystems by Accounting for spatial structures and connectivity”, and ERANETMED3-062 CHAAMS: global
440 Change: Assessment and Adaptation to Mediterranean region water Scarcity.
441

442 **References**

443 Benkirane, M.; Laftouhi, N.-E. ; El Mansouri, B. ; Salik, I. ; Snineh, M. ; El Ghazali, F. E. ; Safia, K. ;
444 Zamrane, Z. An approach for flood assessment by numerical modeling of extreme hydrological events in the
445 Zat watershed (High Atlas, Morocco). *Urban Water Journal*. 2020, 17, 381-389.

446 Bollasina, M.A.; Ming, Y.; Ramaswamy, V. Anthropogenic aerosols and the weakening of the South Asian
447 summer monsoon. *Science* 2011, 334, 502–505.

448 Borga, M.; Anagnostou, E.N.; Blöschl, G.; Creutin, J. Flash Floods: Observations and analysis of hydro-
449 meteorological controls. *J. Hydrol.* 2010, 394, 1–3.

450 Chandrasekar, V.; Le, M. Evaluation of profile classification module of GPM-DPR algorithm after launch. In
451 Proceedings of the IEEE International Geoscience and Remote Sensing Symposium (IGARSS), Milan, Italy,
452 26–31 July 2015; pp. 5174–5177.

453 Chen, C.; Chen, Q.; Duan, Z.; Zhang, J.; Mo, K.; Li, Z.; Tang, G. Multiscale Comparative Evaluation of the
454 GPM IMERG v5 and TRMM 3B42 v7 Precipitation Products from 2015 to 2017 over a Climate Transition
455 Area of China. *Remote Sens.* 2018, 10, 944.



- 456 Duan, Z.; Liu, J.; Tuo, Y.; Chiogna, G.; Disse, M. Evaluation of eight high spatial resolution gridded
457 precipitation products in Adige Basin (Italy) at multiple temporal and spatial scales. *Sci. Total Environ.* 2016,
458 573, 1536–1553.
- 459 Funk, C.; Peterson, P.; Landsfeld, M.; Pedreros, D.; Verdin, J.; Shukla, S.; Michaelsen, J. The climate hazards
460 infrared precipitation with stations—A new environmental record for monitoring extremes. *Sci. Data* 2015, 2,
461 150066.
- 462 Gebregiorgis, A.S.; Kirstetter, P.E.; Hong, Y.; Gourley, J.J.; Huffman, G.J.; Peterson, W.A.; Xue, X.W.;
463 Schwaller, M.R. To what extent is the day 1 GPM IMERG satellite precipitation estimate improved as
464 compared to TRMM TMPA-RT? *J. Geophys. Res. Atmos.* 2018, 123, 1694–1707.
- 465 Germann, U.; Galli, G.; Boscacci, M.; Bolliger, M. Radar precipitation measurement in a mountainous region.
466 *Q. J. R. Meteorol. Soc.* 2006, 132, 1669–1692.
- 467 Guo, J.; Zhai, P.; Wu, L.; Cribb, M.; Li, Z.; Ma, Z.; Wang, F.; Chu, D.; Wang, P.; Zhang, J. Diurnal variation
468 and the influential factors of precipitation from surface and satellite measurements in Tibet. *Int. J. Climatol.*
469 2014, 34, 2940–2956.
- 470 Hou, A.Y.; Kakar, R.K.; Neeck, S.; Azarbarzin, A.A.; Kummerow, C.D.; Kojima, M.; Iguchi, T. The global
471 precipitation measurement mission. *Bull. Am. Meteorol. Soc.* 2014, 95, 701–722.
- 472 Hrachowitz, M.; Weiler, M. Uncertainty of Precipitation Estimates Caused by Sparse Gauging Networks in a
473 Small, Mountainous Watershed. *J. Hydrol. Eng.* 2011, 16, 460–471.
- 474 Huffman, G.J.; Bolvin, D.T.; Nelkin, E.J.; Wolff, D.B.; Adler, R.F.; Gu, G.; Stocker, E.F. The TRMM
475 multisatellite precipitation analysis (TMPA): Quasi-global, multiyear, combined-sensor precipitation
476 estimates at fine scales. *J. Hydrometeorol.* 2007, 8, 38–55.
- 477 Hussain, Y.; Satgé, F.; Hussain, M.B.; Martinez-Carvajal, H.; Bonnet, M.-P.; Cárdenas-Soto, M.; Roig, H.L.;
478 Akhter, G. Performance of CMORPH, TMPA, and PERSIAN rainfall datasets over plain, mountainous, and
479 glacial regions of Pakistan. *Theor. Appl. Climatol.* 2018, 131, 1119–1132.
- 480 Jiang, S.; Liu, S.; Ren, L.; Yong, B.; Zhang, L.; Wang, M.; Lu, Y.; He, Y. Hydrologic Evaluation of Six High-
481 Resolution Satellite Precipitation Products in Capturing Extreme Precipitation and Streamflow over a
482 Medium-Sized Basin in China. *Water* 2017, 10, 25.
- 483 Joyce, R.J.; Janowiak, J.E.; Arkin, P.A.; Xie, P. CMORPH: A Method that Produces Global Precipitation
484 Estimates from Passive Microwave and Infrared Data at High Spatial and Temporal Resolution. *J.*
485 *Hydrometeorol.* 2004, 5, 487–503.
- 486 Kim, K.; Park, J.; Baik, J.; Choi, M. Evaluation of topographical and seasonal feature using GPM IMERG
487 and TRMM 3B42 over Far-east Asia. *Atmos. Res.* 2017, 187, 95–105.
- 488 Liu, Z.; Ostrenga, D.; Vollmer, B.; Deshong, B.; Macritchie, K.; Greene, M.; Kempler, S. Global precipitation
489 measurement mission products and services at the NASA GES DISC. *Bull. Am. Meteorol. Soc.* 2017, 98,
490 437–444.
- 491 Mei, Y.; Anagnostou, E.N.; Nikolopoulos, E.I.; Borga, M. Error Analysis of Satellite Precipitation Products
492 in Mountainous Basins. *J. Hydrometeorol.* 2014, 15, 1778–1793.
- 493 Milewski, A., El Kadiri, R., and Durham, M., 2015, Assessment and Intercomparison of TMPA Satellite
494 Precipitation Products in Varying Climatic and Topographic Regimes in Morocco, *Remote Sensing*, v. 7,
495 5697–5717.



- 496 Milewski, A., Seyoum, W., Elkadiri, R., and Durham, M., 2020, Multi-Scale Hydrologic Sensitivity to
497 Climatic and Anthropogenic Changes in Morocco, *Geosciences*, 10(1), 13
- 498 Palomino-Ángel, S.; Anaya-Acevedo, J.A.; Botero, B.A. Evaluation of 3B42V7 and IMERG daily-
499 precipitation products for a very high-precipitation region in northwestern South America. *Atmos. Res.* 2019,
500 217, 37–48.
- 501 Retalis, A.; Katsanos, D.; Tymvios, F.; Michaelides, S. Validation of the First Years of GPM Operation over
502 Cyprus. *Remote Sens.* 2018, 10, 1520.
- 503 Ringard, J.; Becker, M.; Seyler, F.; Linguet, L. Temporal and spatial assessment of four satellite rainfall
504 estimates over French Guiana and North Brazil. *Remote Sens.* 2015, 7, 16441–16459.
- 505 Rozante, J.R.; Vila, D.A.; Chiquetto, J.B.; Fernandes, A.A.; Alvim, D.S. Evaluation of TRMM/GPM Blended
506 Daily Products over Brazil. *Remote Sens.* 2018, 10, 882.
- 507 Saber, M.; Hamaguchi, T.; Kojiri, T.; Tanaka, K.; Sumi, T. A physically based distributed hydrological model
508 of wadi system to simulate flash floods in arid regions. *Arab. J. Geosci.* 2015, 8, 143–160.
- 509 Scharffenberg, W. A., and M. J. Fleming. 2016. Hydrologic Modeling System HEC-HMS V4.2: User's
510 manual, 614. Davis, CA: US Army Corps of Engineers, Hydrologic Engineering Center
- 511 Sorooshian, S.; Hsu, K.L.; Gao, X.; Gupta, H.V.; Imam, B.; Dan, B. Evaluation of Persian system satellite-
512 based estimates of tropical rainfall. *Bull. Am. Meteorol. Soc.* 2000, 81, 2035–2046.
- 513 Tan, M.L.; Santo, H. Comparison of GPM IMERG, TMPA 3B42 and PERSIAN-CDR satellite precipitation
514 products over Malaysia. *Atmos. Res.* 2018, 202, 63–76.
- 515 Tong, K.; Su, F.; Yang, D.; Hao, Z. Evaluation of satellite precipitation retrievals and their potential utilities
516 in hydrologic modeling over the Tibetan Plateau. *J. Hydrol.* 2014, 519, 423–437.
- 517 Wang, X.; Ding, Y.; Zhao, C.; Wang, J. Similarities and improvements of GPM IMERG upon TRMM 3B42
518 precipitation product under complex topographic and climatic conditions over Hexi region, Northeastern
519 Tibetan Plateau. *Atmos. Res.* 2019, 218, 347–363.
- 520 Wu, L.; Xu, Y.P.; Wang, S.Y. Comparison of TMPA-3B42RT legacy product and the equivalent IMERG
521 products over Mainland China. *Remote Sens.* 2018, 10, 1778.
- 522 Xia, T.; Wang, Z.; Zheng, H. Topography and Data Mining Based Methods for Improving Satellite
523 Precipitation in Mountainous Areas of China. *Atmosphere* 2015, 6, 983–1005.
- 524 Yi, L.; Zhang, W.; Wang, K. Evaluation of heavy precipitation simulated by the WRF model using 4D-Var
525 data assimilation with TRMM 3B42 and GPM IMERG over the Huaihe River basin China. *Remote Sens.*
526 2018, 10, 646.
- 527 Yuan, F.; Zhang, L.; Win, K.W.W.; Ren, L.; Zhao, C.; Zhu, Y.; Jiang, S.; Liu, Y. Assessment of GPM and
528 TRMM multi-satellite precipitation products in streamflow simulations in a data-sparse mountainous
529 watershed in Myanmar. *Remote Sens.* 2017, 9, 302.
- 530 Zhong, R.; Chen, X.; Lai, C.; Wang, Z.; Lian, Y.; Yu, H.; Wu, X. Drought monitoring utility of satellite-based
531 precipitation products across mainland China. *J. Hydrol.* 2019, 568, 343–359.
- 532 Zhu, G.; He, Y.; Pu, T.; Wang, X.; Jia, W.; Li, Z.; Xin, H. Spatial distribution and temporal trends in potential
533 evapotranspiration over Hengduan Mountains region from 1960 to 2009. *J. Geogr. Sci.* 2012, 22, 71–85.
- 534